

Prospect for measurement of CP-violating parameters of $B_s^0 \rightarrow \phi\gamma$ at the Tera Z factory

Hengyu Wang^{1,2} **Hanhua Cui**^{1,2} **Yongfeng Zhu**^{1,2} **Hao Liang**^{1,2} **Yuxin Wang**^{1,2} **Kaili Zhang**^{1,2} **Yi Wang**^{1,2} **Weizheng Song**^{1,2} **Lingfeng Li**³ **Shanzhen Chen***^{1,2} **Manqi Ruan***^{1,2}

¹*Institute of High Energy Physics, Chinese Academy of Sciences
Beijing 100049, China*

²*University of Chinese Academy of Sciences(UCAS)
Beijing 100049, China*

³*International Center of Theoretical Physics-Asia Pacific, University of Chinese Academy of Sciences(UCAS)
Beijing 1000049, China*

E-mail: ruanmq@ihep.ac.cn, szchen@ihep.ac.cn

ABSTRACT:

$b \rightarrow s\gamma$ transition is a critical flavor-changing neutral current (FCNC) process that could be used to probe CP violation (CPV) and new physics (NP). The Circular Electron-Positron Collider (CEPC) offers unique advantages for studying flavor physics, as it provides high statistics, a clean collision environment, and superior detector performance. We quantify the anticipated precision for measuring $B_s^0 \rightarrow \phi\gamma$ at the CEPC Z pole operation, showing that the relative statistical uncertainty could be as low as 0.16%, improved by approximately two orders of magnitude compared to existing measurements. Additionally, we perform a time-dependent analysis of the $B_s^0 \rightarrow \phi\gamma$ decay, accounting for B_s^0/\bar{B}_s^0 mixing extract the mixing-induced and CP-violating parameters $\mathcal{A}_{\phi\gamma}^\Delta$, $\mathcal{C}_{\phi\gamma}$ and $\mathcal{S}_{\phi\gamma}$. Using central value from LHCb measurement as input, we evaluate the anticipated accuracy of measurements of these parameters. The projected statistical uncertainties are $\sigma_{A_{\phi\gamma}^\Delta}^{\text{stat}} = 0.021$, $\sigma_{\mathcal{C}_{\phi\gamma}}^{\text{stat}} = 0.0092$ and $\sigma_{\mathcal{S}_{\phi\gamma}}^{\text{stat}} = 0.0096$, and the systematic uncertainties are $\sigma_{A_{\phi\gamma}^\Delta}^{\text{syst}} = 0.035$, $\sigma_{\mathcal{C}_{\phi\gamma}}^{\text{syst}} = 0.0027$ and $\sigma_{\mathcal{S}_{\phi\gamma}}^{\text{syst}} = 0.0064$. Furthermore, the 1σ sensitivity boundaries for NP in this study are found to be $\mathcal{A}_{\phi\gamma}^\Delta < -0.05$ or $\mathcal{A}_{\phi\gamma}^\Delta > 0.15$, $\mathcal{C}_{\phi\gamma} < -0.02$ or $\mathcal{C}_{\phi\gamma} > 0.04$, and $\mathcal{S}_{\phi\gamma} < -0.04$ or $\mathcal{S}_{\phi\gamma} > 0.04$. We also conduct a relevant detector optimization study by establishing the correlation between the anticipated precision and the intrinsic resolution of the ECAL, as well as the performance of the PID system.

KEYWORDS: Bottom Quarks, Precise Measurement, Flavor-Changing Neutral Currents (FCNC), CP-violating, New Physics

Contents

1	Introduction	1
2	Reference detector, samples, and method	4
3	Events selection and results	6
3.1	Events selection	6
3.1.1	Reconstruction of $\phi \rightarrow K^+K^-$	6
3.1.2	Reconstruction of $B_s^0 \rightarrow \phi\gamma$	9
3.1.3	b tagging	9
3.2	BDT training results	9
4	Detector performance dependence	11
5	Impact of mixing-induced and CP-violating observables	12
5.1	Impact of B_s^0 - \bar{B}_s^0 oscillation	12
5.2	Measurement of CP-violating parameters	15
5.3	Systematic uncertainties	18
5.4	Sensitivity to New Physics	19
6	Conclusion	21

1 Introduction

Flavor-changing neutral current (FCNC) processes serve as a crucial probe of fundamental interactions and are highly important for testing the Standard Model (SM) [1, 2]. FCNC processes in the SM are suppressed due to the off-diagonal elements of the CKM matrix and loop factors, making such decays rare and difficult to detect [3–6]. A significant deviation from SM predictions in FCNC observables often serves as a “smoking gun” for new physics (NP). Therefore, a detailed study of FCNC processes can effectively test the SM and potentially uncover NP beyond the SM.

The radiative $b \rightarrow s\gamma$ transition is an FCNC process. This transition occurs in the SM through one-loop W boson exchange, as shown on the left panel of Figure 1. Potential exchange of new virtual particles in the loop may modify the decay rates and the helicity structure of the vertex, as illustrated on the right panel of Figure 1. The exclusive decay $B_s^0 \rightarrow \phi\gamma$ ¹ proceeds via the radiative $b \rightarrow s\gamma$ transition, and exhibits a unique feature. Unlike many FCNC processes, its SM-predicted branching fraction is not heavily suppressed, with a theoretical estimate of approximately 4×10^{-5} and an uncertainty of

¹The inclusion of charge-conjugate processes is implied throughout, unless stated otherwise.

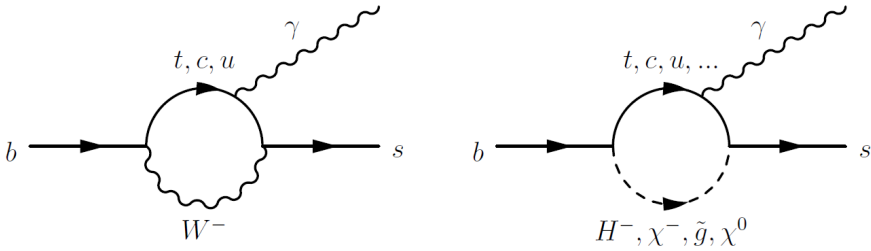


Figure 1. The $b \rightarrow s\gamma$ penguin diagram, mediated by SM particles (left) and new physics particles (right).

about 30% [7, 8]. This makes it accessible to experimental observation and opens a window for precision measurements.

The first experimental observation of this decay was made by the Belle Collaboration in 2008. Based on 23.6 fb^{-1} of $\Upsilon(5S)$ data, the measured branching fraction was $(5.7^{+1.8}_{-1.5}{}^{+1.2}_{-1.1}) \times 10^{-5}$ [9]. Subsequently, the LHCb Collaboration, using 1.0 fb^{-1} of pp collision data, measured the ratio of the branching fractions for $B^0 \rightarrow K^{*0}\gamma$ and $B_s^0 \rightarrow \phi\gamma$ decays and combined it with the world-average value, improving the measurement of $B_s^0 \rightarrow \phi\gamma$ branching fraction to $(3.5 \pm 0.4) \times 10^{-5}$ [10, 11]. Belle further analyzed 121.4 fb^{-1} of $\Upsilon(5S)$ data and obtained a more precise result of $(3.6 \pm 0.5 \pm 0.7) \times 10^{-5}$, which is consistent with the theoretical predictions and with the LHCb results [12, 13]. These experimental results are consistent with the SM description of the $b \rightarrow s\gamma$ process. However, NP scenarios may hide within current measurement uncertainties. To probe such subtle NP effects, sub-percent level precision measurements are essential. The unique advantages of the Circular Electron-Positron Collider (CEPC) in high statistics, clean background, and advanced detector performance make this possible.

Table 1. Expected yields of b-hadrons at Belle II, LHCb Upgrade II, and CEPC Tera-Z.

b-hadrons	Belle II	LHCb (300 fb^{-1})	CEPC(100 ab^{-1})
B^0, \bar{B}^0	5.4×10^{10} (50 ab^{-1} on $\Upsilon(4S)$)	3×10^{13}	4.8×10^{11}
B^\pm	5.7×10^{10} (50 ab^{-1} on $\Upsilon(4S)$)	3×10^{13}	4.8×10^{11}
B_s^0, \bar{B}_s^0	6.0×10^8 (5 ab^{-1} on $\Upsilon(5S)$)	1×10^{13}	1.2×10^{11}
B_c^\pm	-	1×10^{11}	7.4×10^8
$\Lambda_b^0, \bar{\Lambda}_b^0$	-	2×10^{13}	1.0×10^{11}

The primary physics objectives of CEPC are to identify new physics, especially via the Higgs portal. Furthermore, it could be sensitive to new physics through the flavor physics measurements [14]. It is expected to operate for over a decade, including two years at the Z pole. Under an operation scenario of 50 MW synchrotron radiation (SR) power per beam [15], it is expected to produce 4.1×10^{12} Z bosons [15], providing a solid foundation for the precise measurement of rare decays. Owing to various production rates of b-hadrons, CEPC shows significant advantages. Table 1 summarizes the expected numbers of b hadrons produced at Belle II [16], LHCb Upgrade II [17–20], and CEPC Tera-Z [21, 22]. The production yields of B^0/\bar{B}^0 and B^\pm at CEPC are 4.8×10^{11} , approximately an order

of magnitude larger than the corresponding yields at Belle II. Furthermore, the production yields of B_s^0/\bar{B}_s^0 are 1.3×10^{11} , nearly 200 times those of Belle II. For heavier hadrons, such as B_c^\pm and $\Lambda_b/\bar{\Lambda}_b$, CEPC also demonstrates production advantages, with yields of 7.4×10^8 and 1.0×10^{11} , respectively. These abundant hadronic yields will allow the CEPC to accumulate significantly larger data samples for the study of rare b decays [23–26], significantly enhancing the accuracy and reliability of measurements. Compared to LHCb, the e^+e^- collision environment of CEPC features a clean background with negligible pile-up effects [27], greatly reducing backgrounds and further improving measurement precision.

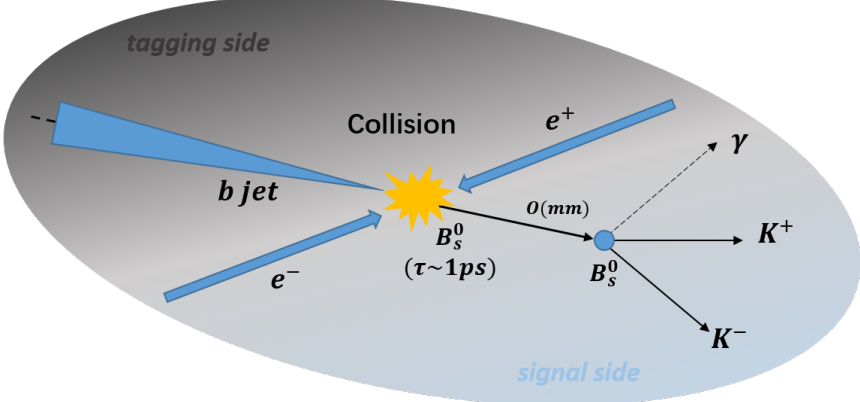


Figure 2. The topology of $B_s^0 \rightarrow \phi\gamma$ decay at Z-pole.

Figure 2 illustrates the decay topology of $B_s^0 \rightarrow \phi(K^+K^-)\gamma$ at the CEPC Z pole. In this scenario, an event is divided into a tagging side and a signal side. The Jet origin identification (JOI) algorithm [28] is applied for b -jet tagging on the tagging side. B_s^0 mesons are produced through the hadronization of a b quark originating from the interaction point (IP) on the signal side. The B_s^0 meson decays into a ϕ meson and a γ photon. The produced ϕ meson subsequently decays into two charged K mesons, i.e., $\phi \rightarrow K^+K^-$. The lifetime of the B_s^0 meson is $(1.527 \pm 0.011) \times 10^{-12} s$. Given an average momentum of approximately 45 GeV, the corresponding flight distance is on the order of $O(mm)$.

The signal efficiency and purity are defined as follows:

$$\epsilon = \frac{\text{Events of correctly reconstructed } B_s^0 \rightarrow \phi\gamma}{\text{Events of all } B_s^0 \rightarrow \phi\gamma} \quad (1.1)$$

$$p = \frac{\text{Events of correctly reconstructed } B_s^0 \rightarrow \phi\gamma}{\text{Total events of reconstructed } B_s^0 \rightarrow \phi\gamma} \quad (1.2)$$

and the relative statistical uncertainty of this decay is defined as $\frac{\sqrt{S+B}}{S}$, which is proportional to $\frac{1}{\sqrt{\epsilon \times p}}$. In this analysis, the event selection criteria are optimized to maximize the measurement precision.

This paper utilizes fast simulation, a cut-based method and boosted decision trees (BDT) [29] to achieve a precise measurement of the relative statistical uncertainty of this process at the CEPC. The remainder of this paper is organized as follows: Section 2 introduces the reference detector, samples, and the fast simulation method. Section 3

presents the detailed event selection strategy, and results from BDT training. Section 4 discusses the correlations between the anticipated precision and detector performance. Section 5 presents the measurement results of the CP-violating parameters derived from a time-dependent analysis of the $B_s^0 \rightarrow \phi\gamma$ decay. Finally, conclusions are drawn in Section 5.

2 Reference detector, samples, and method

This study employs the Marlin fast simulation method [30] based on the CEPC software framework to model detector response based on the performance parameters of the CEPC baseline detector. The core parameters are primarily adopted from the CEPC Conceptual Design Report (CDR) [31]. For charged track reconstruction, the key performance parameters are:

$$\sigma_{r\phi} = 5 \oplus \frac{10}{p(\text{GeV}) \times \sin^{3/2}\theta} \text{ } (\mu\text{m}) \quad (2.1)$$

$$\sigma(1/p_T) = 2 \times 10^{-5} \oplus \frac{0.001}{p(\text{GeV}) \sin^{3/2}\theta} \quad (2.2)$$

Equation 2.1 describes the track vertex reconstruction, and equation 2.2 describes the track transverse momentum reconstruction. For gamma reconstruction, the CEPC CDR scheme employs a Si-W sampling electromagnetic calorimeter [31, 32] with an energy resolution of

$$\frac{\sigma_E}{E} = \frac{17.1\%}{\sqrt{E}} \oplus 1\% \quad (2.3)$$

The CEPC ECAL performance has been studied in recent R&D efforts [33–35]. For instance, a BGO crystal-based ECAL has achieved an energy resolution better than 3% at 1 GeV. Furthermore, the CEPC baseline design includes an excellent particle identification (PID) system. By combining the Time Projection Chamber (TPC) and the Time-of-Flight (TOF) detector, the CEPC is expected to achieve a 3σ separation power for K/π . The detailed PID performance and PID performance matrix is shown in Figure 3 [36].

Table 2. Branching Ratios and Related Factors for $B_s^0 \rightarrow \phi\gamma$ Decays

$Br(Z \rightarrow b\bar{b})$	$(15.12 \pm 0.05)\%$
$f(b \rightarrow B_s^0)$	0.404 ± 0.007
$f(b \rightarrow B_s^0)$	0.101 ± 0.008
$Br(B_s^0 \rightarrow \phi\gamma)$	$(3.4 \pm 0.4) \times 10^{-5}$
$Br(\phi \rightarrow K^+K^-)$	$(49.1 \pm 0.5)\%$

The signal events for $B_s^0 \rightarrow \phi\gamma$ primarily originate from the hadronization process $b \rightarrow B_s^0$. According to existing experimental data, the branching fraction for the Z boson decaying into bottom quark pairs $Z \rightarrow b\bar{b}$ is $(15.12 \pm 0.05)\%$ [37]. Additionally, the fragmentation fraction for $b \rightarrow B_s^0$ is 0.101 ± 0.008 [21], and the branching fraction of $B_s^0 \rightarrow \phi\gamma$ is $(3.4 \pm 0.4) \times 10^{-5}$ [11]. In this study, we reconstruct the ϕ meson using the decay process

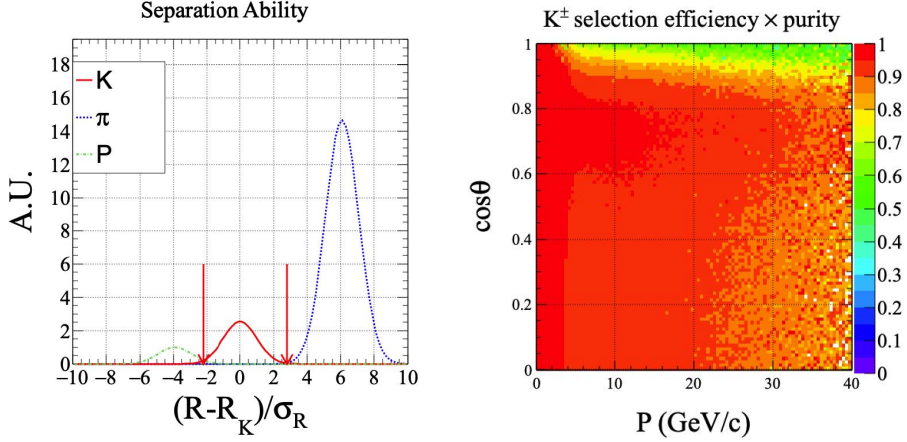


Figure 3. The PID performance by combining dE/dx and TOF at a momentum ranging from 12.0 GeV/c to 12.4 GeV/c and a $\cos\theta$ ranging from 0.30 to 0.31 is shown on the left panel and the performance of K^\pm identification with maximum efficiency times purity at different momentum and cosine polar angle combinations is shown on the right panel.

Table 3. Expected Signals and Background Yields, Sample Sizes, and Their Weights in TeraZ.

Progress	Yield	Samples
$B_s^0 \rightarrow \phi(K^+K^-)\gamma$	1.0×10^6	2.2×10^5
$Z \rightarrow d\bar{d}$	6.5×10^{11}	2.0×10^8
$Z \rightarrow u\bar{u}$	4.6×10^{11}	2.0×10^8
$Z \rightarrow s\bar{s}$	6.5×10^{11}	2.0×10^8
$Z \rightarrow c\bar{c}$	4.9×10^{11}	2.0×10^8
$Z \rightarrow b\bar{b}$	6.2×10^{11}	2.0×10^8

$\phi \rightarrow K^+K^-$. The branching fraction for this decay mode is $(49.1 \pm 0.5)\%$. The relevant branching fractions and fragmentation fractions are listed in Table 2. Therefore, we can estimate the expected number of signal events for the decay $B_s^0 \rightarrow \phi(K^+K^-)\gamma$ as follows:

$$Events_{B_s^0 \rightarrow \phi\gamma} = Z_{yield} \times Br(Z \rightarrow b\bar{b}) \times f(b \rightarrow B_s^0) \times Br(B_s^0 \rightarrow \phi\gamma) \approx 2,128,805$$

$$Events_{B_s^0 \rightarrow \phi(K^+K^-)\gamma} = Events_{B_s^0 \rightarrow \phi\gamma} \times Br(\phi \rightarrow KK) \approx 1,043,124$$

Table 3 summarizes the expected yields and simulated sample sizes of the signals and inclusive $Z \rightarrow q\bar{q}$ background used in this analysis. Both the background and signal Monte Carlo (MC) sample were generated by the Whizard [38] and Pythia [39] packages. Due to the extremely large expected yield at Tera-Z, it is computationally prohibitive to produce all background events. Therefore, we only use 10^9 inclusive $Z \rightarrow qq$ as the background. These samples were generated without $B_s^0 \rightarrow \phi\gamma$ signal events and are categorized according to the quark flavor (d, u, s, c, b).

3 Events selection and results

3.1 Events selection

In the event selection process, the kinematic features and invariant masses of ϕ and B_s^0 candidates are used to distinguish the signal from backgrounds. Subsequently, b-tagging is applied to further suppress background. The detailed selection criteria are outlined below.

Table 4. Cut Chain Results for Signal and Background Candidates

Events	signal	Background		S/B(%)	Accuracy(%)
Cut Chain	$B_s \rightarrow \phi(\rightarrow K^+ K^-) \gamma$ 1.04×10^6	$Z \rightarrow d\bar{d}, u\bar{u}, s\bar{s}$ 1.76×10^{12}	$Z \rightarrow c\bar{c}$ 4.90×10^{11}	Remaining $Z \rightarrow b\bar{b}$ 6.20×10^{11} 3.63×10^{-5}	$\sqrt{S + B}/S$ 162
$K^+ K^-$ Pair Selection	1.04×10^6	6.37×10^{11}	2.38×10^{11}	3.66×10^{11}	8.39×10^{-5} 107
$\log 10(\chi^2) < 1$	9.98×10^5	5.64×10^{11}	1.91×10^{11}	2.43×10^{11}	1.00×10^{-4} 100
$\log 10(V_{\phi \rightarrow K^+ K^-}/\mu m) > 2.6$	7.77×10^5	6.33×10^{10}	4.81×10^{10}	1.39×10^{11}	3.10×10^{-4} 64.5
$1.011 < m_{K^+ K^-} < 1.027 \text{ GeV}$	6.84×10^5	7.39×10^9	8.24×10^9	2.16×10^{10}	1.84×10^{-3} 28.2
$\theta_{\phi\gamma} < 1.0$	6.61×10^5	4.90×10^8	2.21×10^8	1.68×10^8	7.52×10^{-2} 4.49
$E_\gamma > 8 \text{ GeV}$	5.07×10^5	1.81×10^8	3.68×10^7	3.80×10^7	1.99×10^{-1} 3.15
$P_{B_s^0} > 25 \text{ GeV}$	4.59×10^5	1.22×10^7	4.85×10^6	3.27×10^6	2.25×10^0 0.994
$5.187 < m_{\phi\gamma} < 5.547 \text{ GeV}$	4.16×10^5	1.84×10^6	8.16×10^5	4.93×10^5	1.32×10^1 0.454
b-tagging($\epsilon_{b,c,dus \rightarrow b} = 95\%, 1.660\%, 0.065\%$)	3.96×10^5	1.20×10^3	1.36×10^4	4.68×10^5	8.19×10^1 0.237

3.1.1 Reconstruction of $\phi \rightarrow K^+ K^-$

To accurately identify $B_s^0 \rightarrow \phi\gamma$ signal events, we first reconstruct the ϕ meson via its decay $\phi \rightarrow K^+ K^-$. The CEPC's tracking system enables vertex reconstruction with a precision better than $5 \mu m$, much smaller than the millimeter-scale flight distance of B_s^0 mesons. This capability is crucial for suppressing the QCD background, where $\phi \rightarrow K^+ K^-$ pairs are promptly produced at the IP. Vertex reconstruction is performed using the LCFIPlus package [40]. The detailed reconstruction steps for ϕ candidates are as follows:

- 1) Events containing oppositely charged track pairs identified as kaons ($K^+ K^-$) are selected to form ϕ candidates.
- 2) A cut of $\log_{10}(\chi^2) < 1$ is applied. χ^2 is a parameter quantifying the vertex fit quality, calculated as $\chi^2 = \sum_{i=1}^2 \left(\frac{|V_i - V_{\text{fit}}|}{\sigma_i} \right)^2$, where V_{fit} is the fitted vertex position, V_i is the point on one track that is closest to the other, and σ_i is the position uncertainty of the i -th track. This cut ensures high-quality vertex fits.
- 3) A cut of $\log_{10}(\frac{V_{\phi \rightarrow K^+ K^-}}{\mu m}) > 2.6$ is applied. $V_{\phi \rightarrow K^+ K^-}$ represents the decay vertex position of the $\phi \rightarrow K^+ K^-$ decay. Since the ϕ meson originates from a B_s^0 decay, the flight distance of the B_s^0 is on the order of $O(mm)$. Consequently, the decay vertex position for signal ϕ candidates is typically larger than that of background ϕ mesons. The normalized

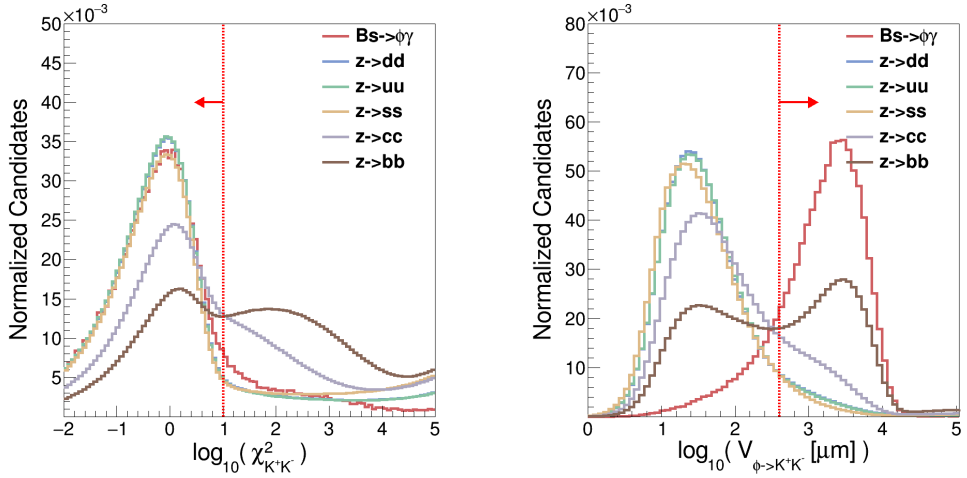


Figure 4. Normalized χ^2 (left) and $V_{\phi \rightarrow K^+ K^-}$ (right) of signal and background distributions. The selected ranges are $\log_{10}(\chi^2) < 1$ and $\log_{10}\left(\frac{V_{\phi \rightarrow K^+ K^-}}{\mu m}\right) > 2.6$.

distributions of χ^2 and $V_{\phi \rightarrow K^+ K^-}$ for signal and background distributions are shown in Figures 4.

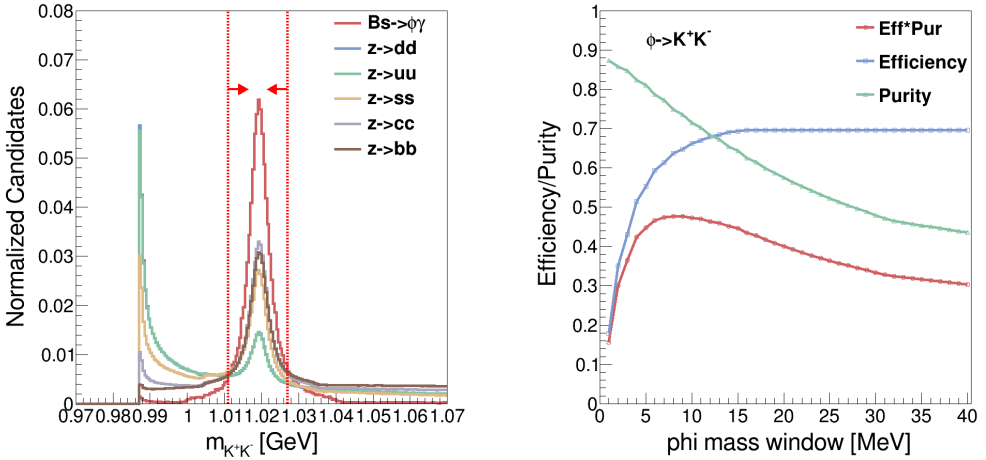


Figure 5. Reconstructed ϕ candidates mass distribution (left) and the overall efficiency and purity distribution (right).

4) A mass window cut of $1.011 < m_{K^+ K^-} < 1.027$ GeV is applied. The reconstructed ϕ candidates mass distribution is shown on the left panel of Figure 5. The efficiency and purity of ϕ reconstruction as functions of the mass window are shown on the right panel

of Figure 5. Where the efficiency ϵ and purity p is defined as follows:

$$\epsilon = \frac{\text{Candidates of correctly reconstructed } \phi \rightarrow K^+ K^-}{\text{Candidates of all } \phi \rightarrow K^+ K^-} \quad (3.1)$$

$$p = \frac{\text{Candidates of correctly reconstructed } \phi \rightarrow K^+ K^-}{\text{Total candidates of reconstructed } \phi \rightarrow K^+ K^-} \quad (3.2)$$

When the ϕ mass window is set to 8 MeV, the optimal $\epsilon \times p$ is achieved. So the reconstructed ϕ candidates within $1.011 < m_{K^+ K^-} < 1.027$ GeV are selected, where the overall reconstruction efficiency and purity for candidate ϕ are 63.6% and 74.9%, respectively. The corresponding efficiency and purity for $B_s^0 \rightarrow \phi \gamma$ signal events at this stage are 69.9% and 98.9%, respectively.

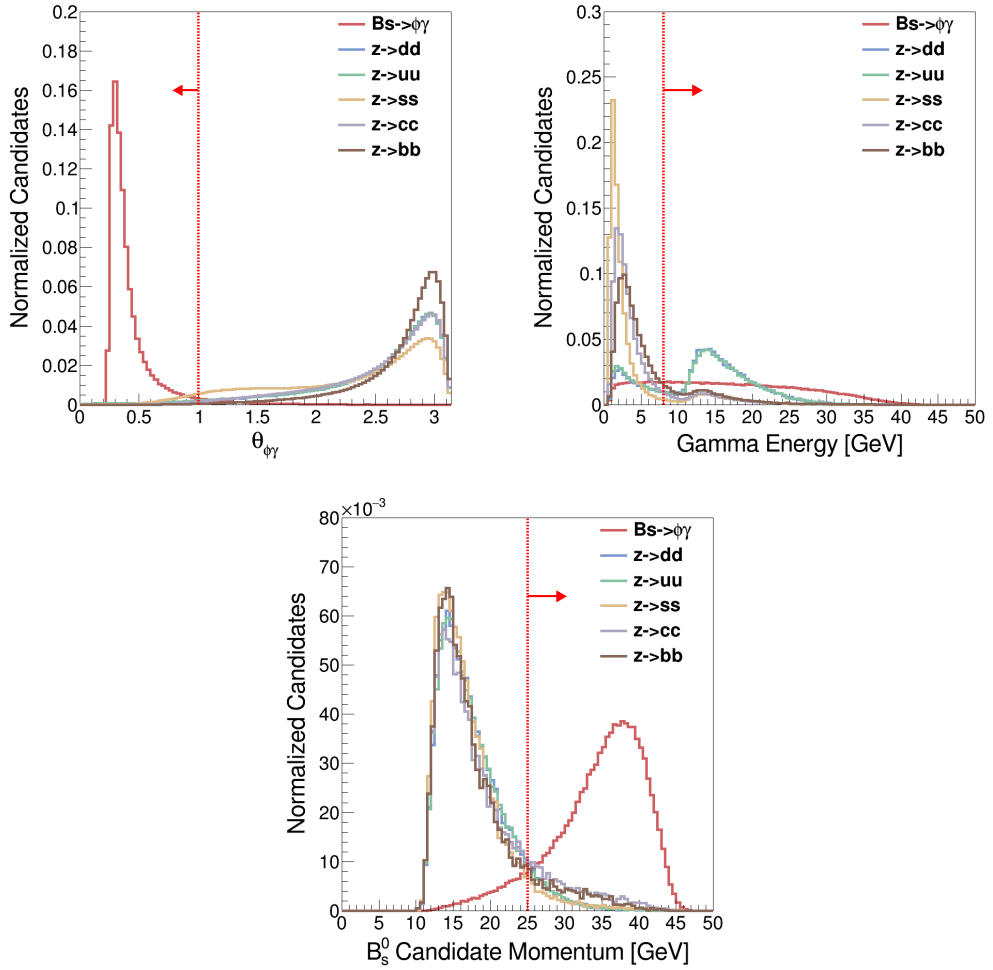


Figure 6. Normalized signal and background distributions for $\theta_{\phi\gamma}$, E_γ , and $P_{B_s^0}$. The selected range are $\theta_{\phi\gamma} < 1.0$, $E_\gamma > 8$ GeV, and $P_{B_s^0} > 25$ GeV.

3.1.2 Reconstruction of $B_s^0 \rightarrow \phi\gamma$

B_s^0 mesons originating from $Z \rightarrow b\bar{b}$ hadronization are expected to have high momentum. Due to the significant boost of the B_s^0 meson, the decay products ϕ and γ are highly collimated. Consequently, both the photon and the reconstructed B_s^0 candidate exhibit relatively high momentum. Therefore, the reconstruction of the B_s^0 candidate proceeds as follows. First, the selected ϕ candidate is paired with a γ to form a B_s^0 candidate. Subsequently, candidates satisfying $\theta_{\phi\gamma} < 1.0$ rad, $E_\gamma > 8$ GeV, $P_{B_s^0} > 25$ GeV are selected. Here, $\theta_{\phi\gamma}$ denotes the opening angle between the $\phi\gamma$ momentum vectors, and the distribution of $\theta_{\phi\gamma}$, E_γ , and $P_{B_s^0}$ are shown on the Figure 6. The B_s^0 invariant mass distribution (before- b -tagging) is obtained, as shown on the left panel of Figure 7. Within the selected mass window $5.187 < m_{\phi\gamma} < 5.547$ GeV, the optimal relative statistical uncertainty reaches $0.443\% \pm 0.0120\%$, with a reconstruction efficiency of 43.9% and a purity of 11.1%. The fitted B_s^0 mass peaks at 5.381 GeV, with a mass resolution of 98.0 MeV.

3.1.3 b tagging

Following the kinematic selections described above, residual backgrounds are dominated by random combinations of a ϕ meson and a photon. Crucially, $B_s^0 \rightarrow \phi\gamma$ decays only occur in b -jets, with no signal events present in uds and c -jets. Consequently, all $\phi\gamma$ combinations reconstructed in uds and c -jets correspond to fake B_s^0 candidates. This key distinction makes b -jet tagging essential for background suppression. As shown in Figure 2, in di-jet events, one jet is used for event selection, and the other is used for jet origin identification. Using the Particle Transformer method [28, 41, 42] at CEPC, b -jet tagging efficiency can reach 95%, with a mis-identification rate of only 0.1% for light quark jets.

Applying b -tagging with 95% efficiency, where the mis-identification rates for c -jets and uds jets are 1.660% and 0.065%, respectively, the invariant mass distribution of the reconstructed B_s^0 candidates is shown in Figure 7. The B_s^0 mass peaks at approximately 5.374 GeV with a mass resolution of 95.0 MeV. Compared with the scenario before b -tagging, the background is significantly suppressed by about 80%, while the signal loss is only about 5%. Within the selected B_s^0 invariant mass window $5.187 < m_{\phi\gamma} < 5.547$ GeV, the optimal measurement relative statistical uncertainty reaches $0.237\% \pm 0.00477\%$, with corresponding efficiency and purity of 41.7% and 43.1%. The complete selection process is summarized in Table 4.

3.2 BDT training results

Following the cut-based selection, we further employ a BDT algorithm to optimize event selection. BDT is better at modeling nonlinear correlations between multiple variables (χ^2 , $V_{\phi \rightarrow KK}$, $m_{K^+K^-}$, $\theta_{\phi\gamma}$, E_γ , $P_{B_s^0}$, $m_{\phi\gamma}$) compared to cut-based method, enabling finer separation between signal and background.

To retain a larger sample of candidate events for BDT training, a pre-selection using a looser cut chain is applied to all signal and background candidates, which is shown in Table 5. The pre-selected events, with b -tagging applied serve as input for BDT training.

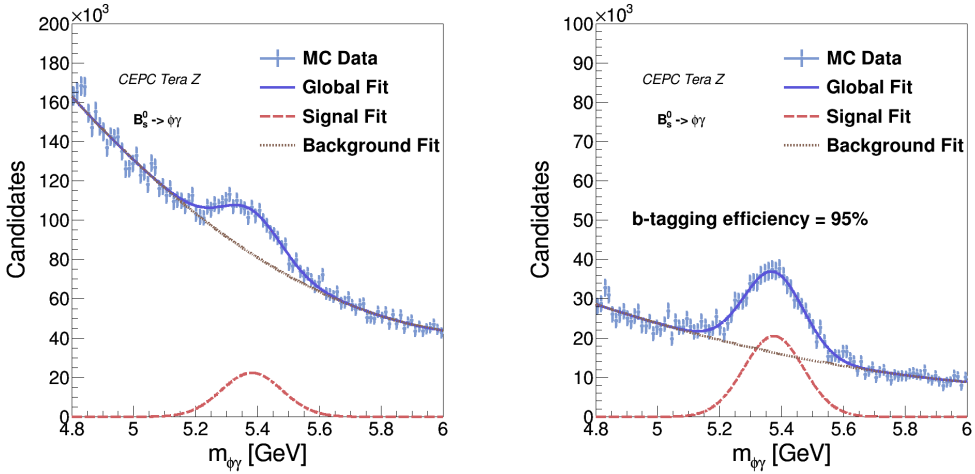


Figure 7. The distribution of the invariant mass of the reconstructed B_s^0 candidates before (left) and after (right) applying b-tagging With a b-tagging efficiency of 95%. The corresponding measurement accuracies are 0.443% and 0.225%, respectively. Note that the data shown are derived from MC samples scaled to 4 TeraZ, the actual statistics correspond to approximately 1/3000 of the displayed counts.

Table 5. The pre-selection cut chain results of signal and background events for BDT

Events	Signal	Background			S/B(%)	Relative Statistical Uncertainty(%)
Cut Chain	$B_s \rightarrow \phi(\rightarrow K^+ K^-) \gamma$ 1.04×10^6	$Z \rightarrow d\bar{d}, u\bar{u}, s\bar{s}$ 1.76×10^{12}	$Z \rightarrow c\bar{c}$ 4.90×10^{11}	$Z \rightarrow b\bar{b}$ 6.20×10^{11}	3.63×10^{-5}	$\sqrt{S + B}/S$ 162
$K^+ K^-$ Pair Selection	1.04×10^6	6.37×10^{11}	2.38×10^{11}	3.66×10^{11}	8.39×10^{-5}	107
$\log 10(\chi^2) < 1$	9.98×10^5	5.64×10^{11}	1.91×10^{11}	2.43×10^{11}	1.00×10^{-6}	100
$\log 10(V_{\phi \rightarrow KK}/\mu m) > 2.1$	9.23×10^5	1.46×10^{11}	8.53×10^{10}	1.71×10^{11}	2.30×10^{-6}	68.7
$1.01 < m_{K^+ K^-} < 1.07 \text{ GeV}$	8.89×10^5	3.89×10^{10}	2.09×10^{10}	4.17×10^{10}	8.75×10^{-6}	35.9
$\theta_{\phi\gamma} < 1.5$	8.77×10^5	5.54×10^9	2.05×10^9	1.86×10^9	9.29×10^{-5}	11.1
$E_\gamma > 5 \text{ GeV}$	7.43×10^5	2.00×10^9	4.07×10^8	4.10×10^8	2.64×10^{-4}	7.13
$P_{B_s^0} > 10 \text{ GeV}$	7.39×10^5	1.51×10^9	2.79×10^8	2.40×10^8	3.64×10^{-4}	6.10
$5.0 < m_{\phi\gamma} < 5.7 \text{ GeV}$	7.32×10^5	5.67×10^8	9.98×10^7	8.48×10^7	9.74×10^{-4}	3.75
b-tagging($\epsilon_{b,c,dus \rightarrow b} = 95\%, 1.660\%, 0.065\%$)	6.96×10^5	3.68×10^5	1.66×10^6	8.06×10^7	8.42×10^{-3}	1.31
BDT Response > 0.24	4.65×10^5	273	4.96×10^3	5.60×10^4	759	0.156

Figure 8 illustrates the BDT response distributions for both signal and background. Applying an optimized cut on the BDT response at 0.24, the remaining signal and background event counts are 465,092 and 61,215, respectively. The achieved selection efficiency and purity are 44.91% and 76.20%, respectively. This yields a final relative statistical uncertainty of $0.156 \pm 0.0025\%$, representing a approximately 32% improvement over the cut-based method and an enhancement of two orders of magnitude compared to existing

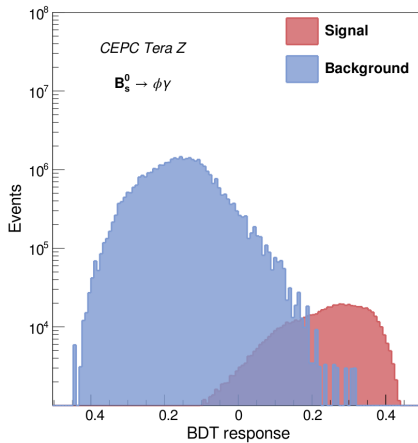


Figure 8. BDT response distributions compared for signal and background after pre-selection and b-tagging. The pre-selection conditions are $\log 10(\chi^2) < 1$, $\log 10(V_{\phi \rightarrow KK}/\mu m) > 2.1$, $1.01 < m_{K^+K^-} < 1.07 \text{ GeV}$, $\theta_{\phi\gamma} < 1.5$, $E_\gamma > 5 \text{ GeV}$, $P_{B_s^0} > 10 \text{ GeV}$, $5.0 < m_{\phi\gamma} < 5.7 \text{ GeV}$

experimental results [11].

4 Detector performance dependence

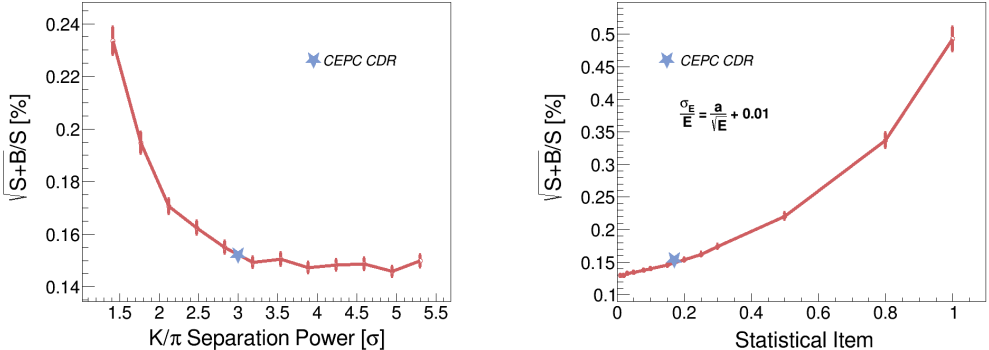


Figure 9. Dependency of $B_s^0 \rightarrow \phi\gamma$ relative statistical uncertainty on PID performance (left) and ECAL resolution (right)

For the measurement of $B_s^0 \rightarrow \phi\gamma$, the presence of charged final-state particles makes the PID performance of the tracker crucial for the overall precision. Figure 9 (left) illustrates the dependence of the relative statistical uncertainty of measurement on the K/π separation power². As K/π separation power improves, the uncertainty improves overall. When K/π separation power is below 3σ , the expected relative statistical uncertainty

²The x-axis is K/π separation power, which is defined as $S_{AB} = \frac{|I_A - I_B|}{\sqrt{\sigma_A^2 + \sigma_B^2}}$. The separation power of K/π is correlated with the separation power of K/p . In this study, we directly take the separation power of K/p to be half of that of K/π .

drops rapidly with increased PID performance. Once the separation power reaches 3σ , the relative statistical uncertainty stabilizes at approximately 0.16%. Further improving PID performance to a near-ideal state marginally improves to about 0.145%, indicating a diminishing returns beyond the 3σ K/π separation power. This result indicates that a 3σ K/π separation power is sufficient to meet the requirements of high-precision measurements, providing a reasonable and effective performance benchmark for the detector design.

Another critical factor affecting the measurement is ECAL energy resolution due to the presence of a photon in the final state. Generally, ECAL resolution can be parameterized by $\frac{\sigma_E}{E} = \frac{a}{\sqrt{E}} \oplus b$, where a is the stochastic term and b is the constant term.³ To study its impact, we vary the stochastic term a from 0 to 1 while keeping the constant term fixed at $b = 0.01$. Figure 9 (right) illustrates the dependence of the measurement precision on the ECAL energy resolution. As ECAL energy resolution improves, the relative statistical uncertainty improves. For the baseline resolution of $\frac{17.1\%}{\sqrt{E}} \oplus 1\%$, and with 3σ K/π separation, the precision is 0.156%. If the resolution improves to 3%, the relative statistical uncertainty improves to 0.133%. Notably, pushing the resolution to a near-ideal state, only yields a marginal further improvement to about 0.129%.

5 Impact of mixing-induced and CP-violating observables

5.1 Impact of B_s^0 - \bar{B}_s^0 oscillation

In the SM, photons in the $b \rightarrow s\gamma$ process are expected to be purely left-handed, a consequence of the W boson's coupling to left-handed quarks (or right-handed antiquarks). However, NP contributions could introduce right-handed helicity photons, while challenging to measure directly, these contributions can be probed indirectly through time-dependent studies of B_s^0 and \bar{B}_s^0 radiative decays [43].

In $B_s^0 \rightarrow \phi\gamma$ decays, the interference between B_s^0 mixing and decay amplitudes modulates the decay rate as a function of proper time [44]. This time dependence is described by [45]:

$$\mathcal{P}(t) \propto e^{-\Gamma_s t} \left\{ \cosh\left(\frac{\Delta\Gamma_s t}{2}\right) - \mathcal{A}^\Delta \sinh\left(\frac{\Delta\Gamma_s t}{2}\right) + \zeta \mathcal{C} \cos(\Delta m_s t) - \zeta \mathcal{S} \sin(\Delta m_s t) \right\} \quad (5.1)$$

where $\Delta\Gamma_s = 0.084 \pm 0.005$ ps $^{-1}$ [21] and $\Delta m_s = 17.765 \pm 0.006$ ps $^{-1}$ [21] are the width and mass differences between the B_s^0 mass eigenstates, $\Gamma_s = 0.6598 \pm 0.0025$ ps $^{-1}$ [21] is the mean decay width, where $\zeta = +1$ (-1) corresponds to an initial B_s^0 (\bar{B}_s^0). The coefficients \mathcal{A}^Δ , \mathcal{C} and \mathcal{S} are functions of the left- and right-handed photon polarization amplitudes [45]. The coefficients \mathcal{A}^Δ and \mathcal{S} are sensitive to the photon helicity amplitudes and weak phases, while \mathcal{C} characterizes direct CP violation. The SM predicts small values for these parameters $\mathcal{A}_{\text{SM}}^\Delta = 0.047^{+0.029}_{-0.025}$, $\mathcal{S}_{\text{SM}} = 0 \pm 0.002$, and $\mathcal{C}_{\text{SM}} \approx 0.005 \pm 0.005$ [45], reflecting the expected minimal CP violation and dominant left-handed photon helicity in the SM. The

³In practice, the ECAL energy resolution also includes a noise term $\frac{c}{E}$, where c arises from the noise superposition of readout electronics channels. Typically, this term can be made very small or even negligible through low-noise electronic design and baseline subtraction, hence it is not included in the parameterization here.

LHCb collaboration has measured these parameters using approximately 5000 $B_s^0 \rightarrow \phi\gamma$ signal events, yielding [46, 47]: $\mathcal{S}_{\phi\gamma} = 0.43 \pm 0.30 \pm 0.11$, $\mathcal{C}_{\phi\gamma} = 0.11 \pm 0.29 \pm 0.11$, and $\mathcal{A}_{\phi\gamma}^{\Delta} = -0.67^{+0.37}_{-0.41} \pm 0.17$. However, limited by the available statistics and flavor-tagging efficiency, LHCb did not observe a clear oscillatory pattern in the decay time distribution, resulting in large statistical uncertainties, precluding definitive tests of the SM. In contrast, the CEPC, with its high-statistics B_s^0 samples and superior flavor-tagging performance, is expected to improve the measurement precision of \mathcal{A}^{Δ} , \mathcal{C} , and \mathcal{S} .

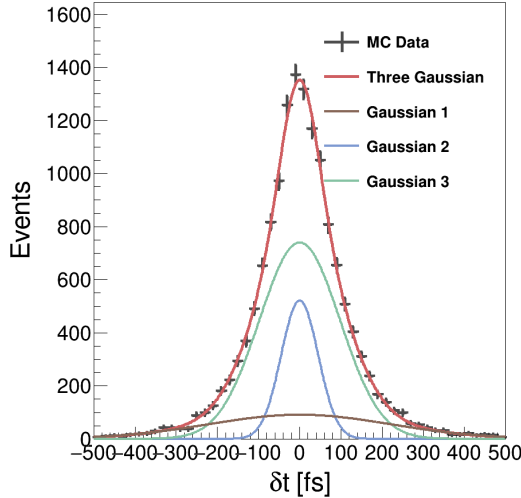


Figure 10. The reconstructed B_s^0 lifetime resolution distribution from full simulation, modeled as a mixture of three Gaussian functions achieving an effective resolution of $\sigma_t = 76\text{ fs}$.

A flavor-tagging algorithm [44] is applied to identify the initial flavor of the B_s^0 meson. The reconstructed B_s^0 candidates can be categorized into correctly tagged (R), incorrectly tagged (W), and untagged (U). The flavor-tagging efficiency, defined as the fraction of events with a flavor tag decision, is $\epsilon_{tag} = \frac{R+W}{R+W+U} = 72.12\%$. The fraction of events that resulted in a wrong decision is referred to mis-tag, which is calculated as $\omega = \frac{W}{R+W} = 21.39\%$. The effective tagging efficiency, or tagging power, defined as $\epsilon_{eff} = \epsilon_{tag}(1 - 2\omega)^2$, is calculated to be 23.60%.

The lifetime of B_s^0 mesons is derived from the reconstructed vertex position and transverse momentum of the B_s^0 candidate, following the relation:

$$\tau = \frac{m_s l_{xy}}{p_T} \quad (5.2)$$

where τ is the reconstructed lifetime of the B_s^0 decay, m_s is its reconstructed mass, l_{xy} is the projected decay length in the transverse plane, p_T is reconstructed transverse momentum. The distribution of reconstructed B_s^0 decay time residual $\delta t = t_{reco} - t_{truth}$ is shown in Figure 10, where the reconstructed time are obtained from full simulation. The nominal value of the decay time error is derived from a fit using three Gaussian functions, which

are combined into an effective resolution $\sigma_t = 76\text{fs}$ following the function:

$$\sigma_t = \sqrt{-\frac{2}{\Delta m_s^2} \ln f_1 e^{-\frac{1}{2}\sigma_1^2 \Delta m_s^2} + f_2 e^{-\frac{1}{2}\sigma_2^2 \Delta m_s^2} + f_3 e^{-\frac{1}{2}\sigma_3^2 \Delta m_s^2}} \quad (5.3)$$

where $f_{1,2,3}$ are the fractional contributions of each Gaussian component, and $\sigma_{1,2,3}$ are their respective widths. The reconstruction efficiency depends on the B_s^0 decay time. Events with decay times that are either too short or too long exhibit reduced efficiencies. This time-dependent efficiency is parameterized by an acceptance function:

$$A(t) = \frac{\alpha t^\beta}{1 + \alpha t^\beta} \times (1 - \xi t) \quad (5.4)$$

where the parameters $\alpha = 4.58$, $\beta = 0.89$, and $\xi = 0.09$, are obtained by fitting selected signal MC events.

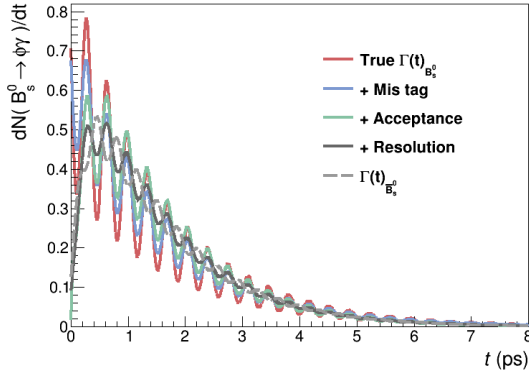


Figure 11. The decay time distribution of $B_s^0 \rightarrow \phi\gamma$ at CEPC.

The expected decay time distribution for $B_s^0 \rightarrow \phi\gamma$ at CEPC is illustrated in Figure 11. This distribution is modeled by a weighted theoretical time-dependent decay rate probability density function (PDF) from Eq 5.1, convolved with the decay time resolution function and an acceptance function. The red line corresponds to the ideal theoretical distribution of decay time for B_s^0/\bar{B}_s^0 oscillation in the absence of detector effects. After introducing flavor-tagging efficiency and mistag probability into the PDF, the B_s^0 decay time distribution corresponds to the blue line in Figure 11. Subsequently, by convolving with the acceptance function described in Eq 5.4, we obtain the decay time distribution described by the green line. By further convolving with a Gaussian distribution with $\sigma_t = 76\text{fs}$, we obtain the final distribution shown as the black line in Figure 11. The decay time spectrum of \bar{B}_s^0 is depicted by the brown dashed line in Figure 11. This final distribution represents the expected observed decay time spectrum at the CEPC.

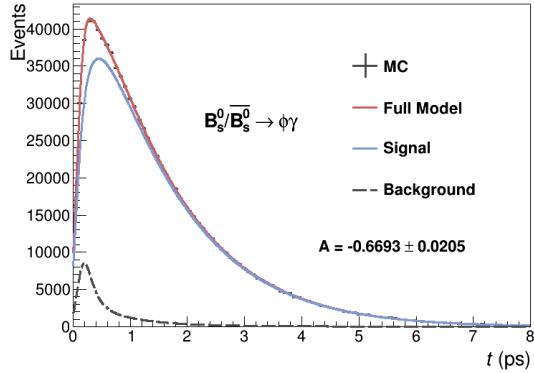


Figure 12. The decay time distribution for untagged $B_s^0 \rightarrow \phi\gamma$ decay time and the single measurement result of parameter A, where fitted $A = -0.67 \pm 0.021$.

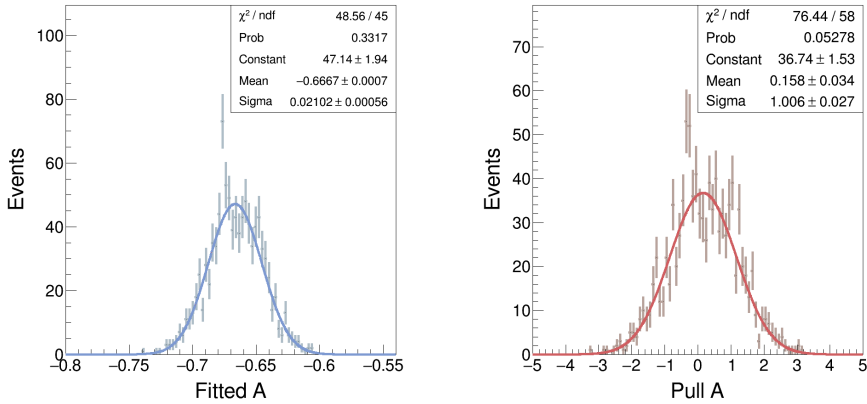


Figure 13. The distribution of fitted value A and pull A for untagged $B_s^0 \rightarrow \phi\gamma$ from 1000 pseudo experiments with generated $A = -0.67$, where $\text{pull } A = \frac{A_{\text{fitted}} - A_{\text{generated}}}{\sigma_A}$.

5.2 Measurement of CP-violating parameters

The CP-violating parameter $A_{\phi\gamma}^{\Delta}$ can be extracted from untagged B_s^0/\bar{B}_s^0 decays. In untagged samples, the initial flavor of B_s^0/\bar{B}_s^0 is unknown, and $C_{\phi\gamma}$, $S_{\phi\gamma}$ cancel out when averaging over B_s^0 and \bar{B}_s^0 events. This cancellation eliminates the need for flavor tagging and simplifies the decay time probability density function (PDF) to a form sensitive only to $A_{\phi\gamma}^{\Delta}$.

$$\mathcal{P}_{\text{untagged}}(t) \propto e^{-\Gamma_s t} \left\{ \cosh\left(\frac{\Delta\Gamma_s t}{2}\right) - A_{\phi\gamma}^{\Delta} \sinh\left(\frac{\Delta\Gamma_s t}{2}\right) \right\} \quad (5.5)$$

To validate the extraction procedure for $A_{\phi\gamma}^{\Delta}$ and quantify potential biases and uncertainties, we generated 930184⁴ Monte Carlo $B_s^0/\bar{B}_s^0 \rightarrow \phi(\rightarrow K^+K^-)\gamma$ events—accounting

⁴In section 3, the selected signal and background yields are 465,092 and 61,217, respectively. While the signal here is the unflavored B_s^0/\bar{B}_s^0 . Since the untagged analysis combines B_s^0 and \bar{B}_s^0 the effective signal

for 44.91% of the total unflavored signal sample size—and 61,217 Monte Carlo background events. The signal events are generated from a combined time dependence distribution described by Eq. 5.5 with acceptance function described by Eq. 5.4 and time resolution incorporated. The input value is set to $A_{\phi\gamma}^{\Delta} = -0.67$, matching the central value of the LHCb measurement. The background events are sampled from an empirical decay time distribution, described by the function

$$\mathcal{P}_{\text{Bkg}}(t) = 0.516 \exp\left(-\frac{1}{2} \times \left(\frac{\ln(\frac{t}{0.155})}{0.578}\right)^2\right) + 0.103 \exp\left(-\frac{1}{2} \times \left(\frac{\ln(\frac{t}{0.427})}{0.833}\right)^2\right) \quad (5.6)$$

This empirical function is derived by fitting the decay time distribution of the selected background events described in Section 3. The decay time distribution of the combined MC signal and background sample, along with fits, is presented in Figure 12. We perform multiple independent pseudo-experiments by repeatedly fitting the combined MC samples. The distribution of fitted A is shown in the left panel of Figure 13. From this distribution, the mean fitted value is fitted $A = -0.6667$ and statistical uncertainty per fit is estimated as $\sigma_{A_{\phi\gamma}^{\Delta}} = 0.021$. The pull quantifies the bias between the fitted result and the true value, which is defined as $\text{pull} = \frac{x_{\text{fitted}} - x_{\text{generated}}}{\sigma_{\text{fitted}}}$, where x_{fitted} is the fitted value, $x_{\text{generated}}$ is its generated value, and σ_{fitted} is the fitting uncertainty of x_{fitted} . The distribution of pull A is shown in the right panel of Figure 13. The central value is 0.16, indicating that the bias of fitted A is within a reasonable range.

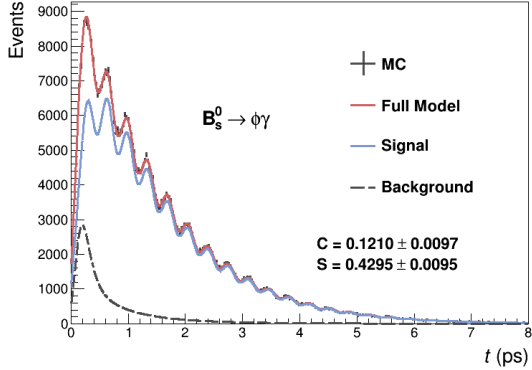


Figure 14. The decay time distribution and corresponding fits for tagged $B_s^0 \rightarrow \phi\gamma$ at CEPC, the measurement result of parameter C and S are $C_{\phi\gamma} = 0.12 \pm 0.0092$ and $S_{\phi\gamma} = 0.43 \pm 0.0096$.

The CP-violating parameters $\mathcal{C}_{\phi\gamma}$ and $\mathcal{S}_{\phi\gamma}$ require flavor-tagged samples due to B_s^0 oscillation and can be extracted from flavor tagged B_s^0/\bar{B}_s^0 decays. We combined Eq. 5.1 with flavor tagging efficiency, acceptance Eq. 5.4 and time resolution, generated 465,092 Monte Carlo $B_s^0 \rightarrow \phi(\rightarrow K^+K^-)\gamma$ events—accounting for 44.91% of the total flavored signal sample size—and 61,217 Monte Carlo background events. The signal events are generated with input values $A_{\phi\gamma}^{\Delta} = -0.67$, $C_{\phi\gamma} = 0.11$, and $S_{\phi\gamma} = 0.43$. The decay

statistics are doubled to 930,184.

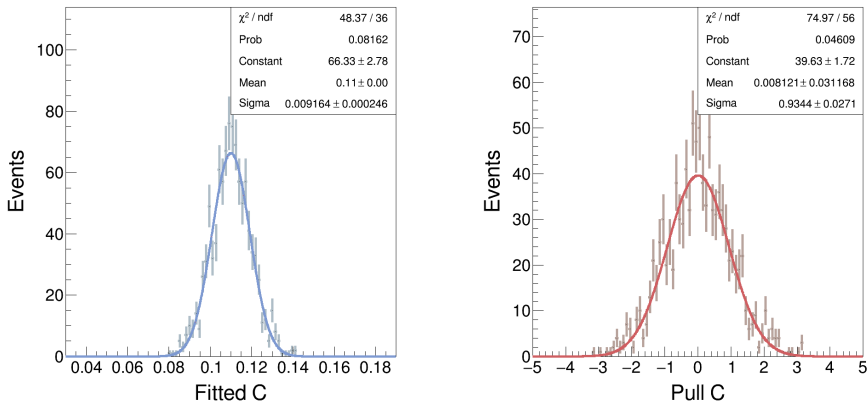


Figure 15. The distribution of fitted value C and pull C for tagged $B_s^0 \rightarrow \phi\gamma$ from 1000 pseudo experiment with generated $C = 0.11$, where pull $C = \frac{C_{\text{fitted}} - C_{\text{generated}}}{\sigma_C}$.

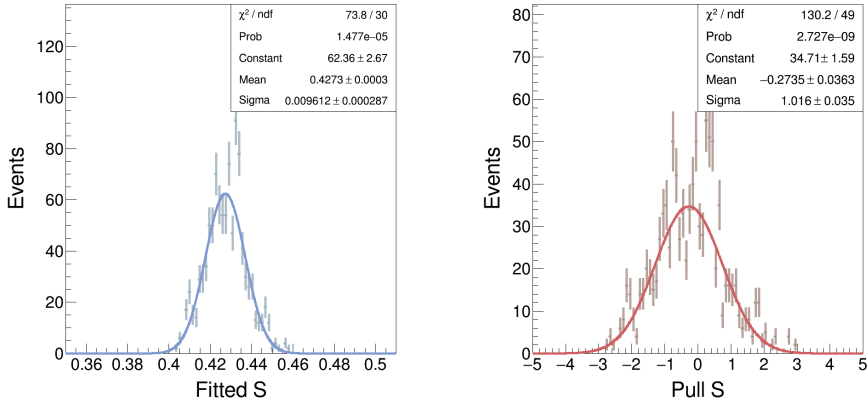


Figure 16. The distribution of fitted value S and pull S for tagged $B_s^0 \rightarrow \phi\gamma$ from 1000 pseudo experiment with generated $S = 0.43$, where pull $S = \frac{S_{\text{fitted}} - S_{\text{generated}}}{\sigma_S}$.

time distribution of the combined MC signal and background sample, along with fits, is presented in Figure 14. We perform 1000 independent pseudo-experiments on statistically independent samples obtained from the same MC distributions. The distribution of fitted C and S are shown in the left panel of Figure 15 and Figure 16, respectively. The statistical uncertainty of $C_{\phi\gamma}$ and $S_{\phi\gamma}$ are $\sigma_C^{\text{stat}} = 0.0092$ and $\sigma_S^{\text{stat}} = 0.0096$. The distribution of pull C and pull S are shown in the right panel of Figure 15 and Figure 16, respectively, the result shown that the bias of fitted C and S are within a reasonable range.

Figure 17 summarizes the statistical uncertainty of C_{CP} and S_{CP} in $b \rightarrow s\gamma$ transitions. The cyan markers indicate the measurement result from BABAR Collaboration [48–50]. The blue markers indicate the measurement result from Belle Collaboration [51–54]. The lilac markers indicate the measurement result from LHCb Collaboration [46]. The red markers show the CEPC Tera-Z anticipated uncertainty obtained from this work. To make the small statistical uncertainties visible, the error bars for CEPC are magnified by a

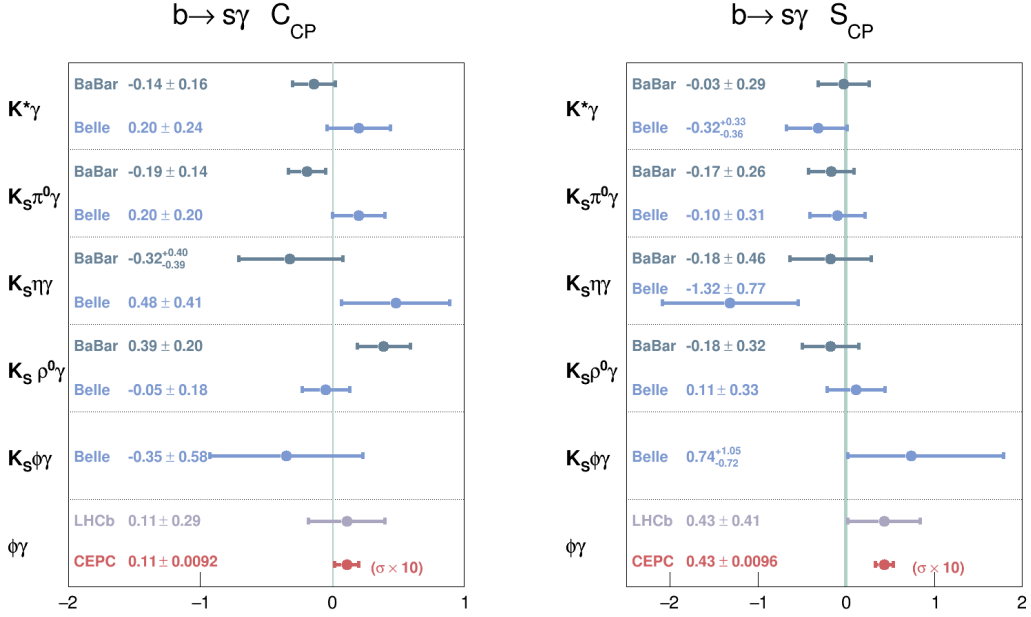


Figure 17. Summary of the C_{CP} and S_{CP} statistical uncertainty in $b \rightarrow s\gamma$ transitions. To clearly visualize the fine statistical uncertainty of CEPC’s measurements, the error bar for CEPC is magnified by a factor of 10.

factor of 10. The SM predictions are indicated by the green band for comparison. The projected CEPC Tera-Z results show significantly smaller uncertainties than those from the B-factories, demonstrating the potential for a significant improvement in precision.

5.3 Systematic uncertainties

The systematic contributions are evaluated by repeating the fit with varying inputs and taking the observed shifts in the fitted values of $\mathcal{A}^{\Delta}, \mathcal{C}, \mathcal{S}$ as the corresponding systematic contribution. A summary of the relevant systematic uncertainties is presented in Table 6

Table 6. Summary of the systematic uncertainties in the analysis of $B_s^0 \rightarrow \phi\gamma$ decays.

Source of Uncertainty	$\sigma(\mathcal{A})$	$\sigma(\mathcal{C})$	$\sigma(\mathcal{S})$
PDF parameters	Γ_s	0.0026	0.00064
	$\Delta\Gamma_s$	0.0025	0.00059
	Δm_s	0	0.00029
Detector	Acceptance	0.021	0.00018
	Time Resolution	0.0062	0.00034
	Initial flavor tag	0	0.00055
Background subtraction	Background	0.0021	0.00009
Total	$\sigma_{\text{syst.}}$	0.035	0.0027
			0.0064

Considering the systematic uncertainties, using central value from LHCb as inputs,

the anticipated result for CP-violating parameters can be expressed as:

$$\begin{aligned}\mathcal{A}_{\phi\gamma}^{\Delta} &= -0.67 \pm 0.021(\text{stat}) \pm 0.035(\text{syst}), \\ \mathcal{C}_{\phi\gamma} &= 0.11 \pm 0.0092(\text{stat}) \pm 0.0027(\text{syst}), \\ \mathcal{S}_{\phi\gamma} &= 0.43 \pm 0.0096(\text{stat}) \pm 0.0064(\text{syst}).\end{aligned}$$

The total uncertainties, obtained by adding the statistical and systematic components in quadrature, are estimated to be $\mathcal{A}_{\phi\gamma}^{\Delta}$, $\mathcal{C}_{\phi\gamma}$, and $\mathcal{S}_{\phi\gamma}$ are $\sigma_{\mathcal{A}_{\phi\gamma}^{\Delta}} = 0.041$, $\sigma_{\mathcal{C}_{\phi\gamma}} = 0.010$ and $\sigma_{\mathcal{S}_{\phi\gamma}} = 0.012$. These represent an improvement of approximately one order of magnitude compared to the latest LHCb results [46, 47].

5.4 Sensitivity to New Physics

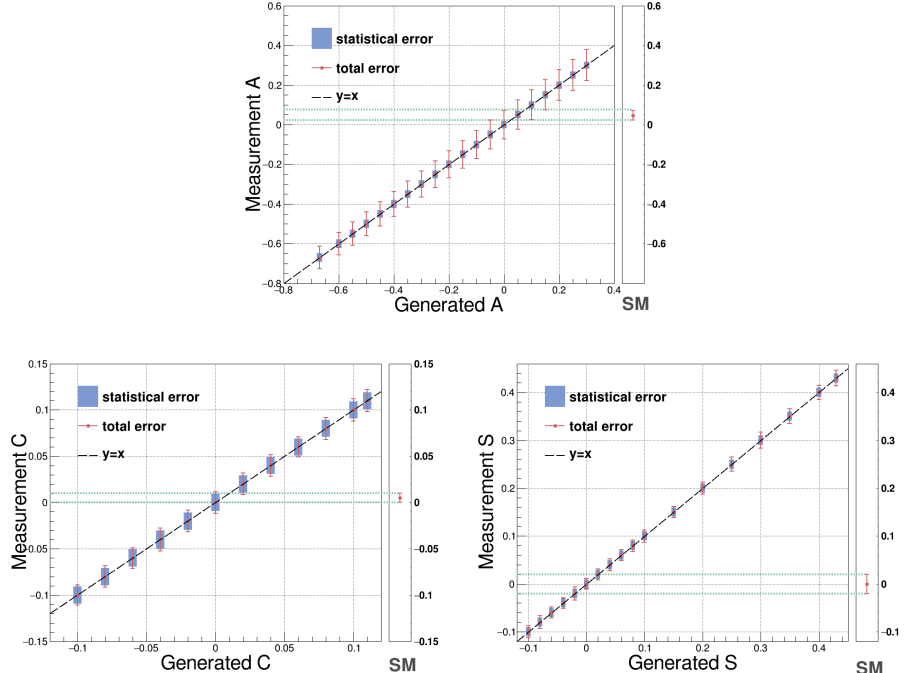


Figure 18. Sensitivity of \mathcal{A}^{Δ} , \mathcal{C} , and \mathcal{S} . The blue rectangular area represents the statistical uncertainty, while the red solid line indicates the total uncertainty, which combines systematic uncertainty and the statistical uncertainty. The green area shows the predicted range by SM.

To investigate the CEPC’s sensitivity to potential NP contributions, we performed a parameter scan over \mathcal{A}^{Δ} , \mathcal{C} , and \mathcal{S} . The results are illustrated in Figure 18. In this figure, for each generated parameter value, blue rectangular bands represent statistical uncertainties, whereas solid red lines represent total uncertainties, i.e., statistical and systematic added in quadrature. Dashed green lines mark the range predicted by the SM. When the true parameter values correspond to the SM predictions, the projected total uncertainties for \mathcal{A}^{Δ} and \mathcal{C} are larger than the current theoretical uncertainties. However, for \mathcal{S} , the projected precision is comparable to the SM theoretical uncertainty. The projected 1σ

sensitivity boundaries for detecting a deviation from the SM are defined as: $\mathcal{A}_{\phi\gamma}^\Delta < -0.05$ or $\mathcal{A}_{\phi\gamma}^\Delta > 0.15$; $\mathcal{C}_{\phi\gamma} < -0.02$ or $\mathcal{C}_{\phi\gamma} > 0.04$; and $\mathcal{S}_{\phi\gamma} < -0.04$ or $\mathcal{S}_{\phi\gamma} > 0.04$. This implies that although the experimental precision for these CP-violating parameters may not yet fully match the theoretical precision of the SM predictions, signatures of NP could still be detected if the measured values lie outside the bounds quoted above.

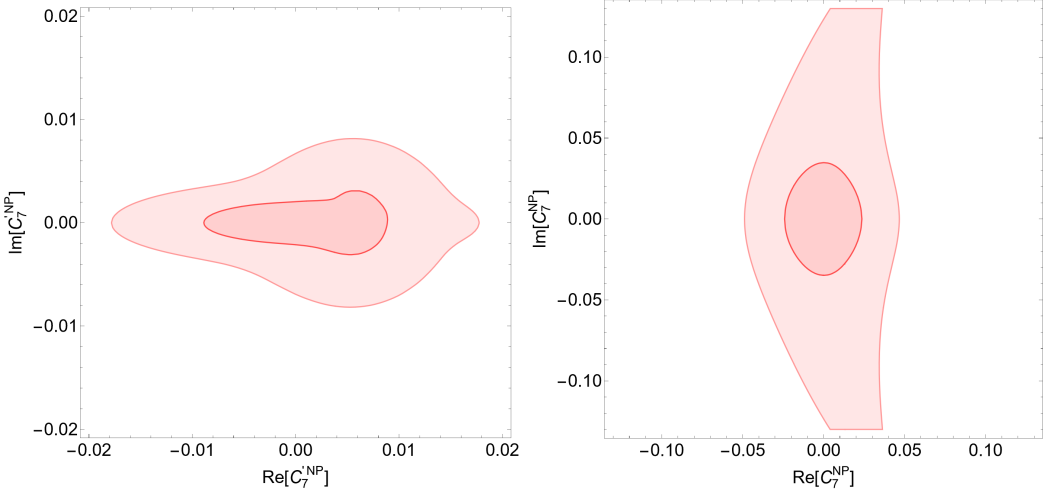


Figure 19. Frequentist constraints on New Physics contributions to the complex Wilson coefficients $C_7^{\prime\text{NP}}$ (left) and C_7^{NP} (right). In both panels we take the SM as our benchmark and the overall uncertainties shown in Section 5.3. Note the two plots have different ranges.

The CP-conserving and CP-violating parameters measured are useful in constraining Wilson coefficients of effective theory (EFT) operators. For example, by comparing the prediction of the SM and experimental uncertainty, the expected sensitivities of $B_s^0 \rightarrow \phi\gamma$ decays at the Tera-Z factory can be used to impose constraints on low energy EFT (LEFT) operators, as well as constraints on UV New Physics contributions [6, 55–58]. In this work, we focus on the NP contribution to the operator $\mathcal{O}_7^{(i)}$, which are defined as

$$\mathcal{H}_{\text{eff}} \supset \frac{4G_F V_{tb} V_{ts}^*}{\sqrt{2}} \left[C_7 \left(\frac{em_b}{16\pi^2} \bar{s}_L \sigma_{\mu\nu} b_R \right) + C'_7 \left(\frac{em_b}{16\pi^2} \bar{s}_R \sigma_{\mu\nu} b_L \right) \right] F^{\mu\nu} + \dots \quad (5.7)$$

where G_F is the Fermi constant and the omitted terms include other FCNC operators. In the SM, C_7 is generated at the leading order while C'_7 is helicity suppressed and therefore smaller by a factor of $\mathcal{O}(m_s/m_b)$. At higher loop order, the four-fermion operators also contribute to the effective value of C_7 (C_7^{eff}) [59], leaving considerable theoretical uncertainties for the calculation of C_7 . The time-dependent CPV measurement on \mathcal{C} and \mathcal{S} is less sensitive to the (soft) hadronic contributions above, allowing a better decision of $\text{Re}(C'_7/C_7)$ and $\text{Im}(C'_7/C_7)$. Since a global fit involving other $b \rightarrow s$ transition measurements is beyond the scope of this work, we take a simplified approach instead and fit the NP contribution to C_7 and C'_7 separately. In each fit, the NP contribution to another is fixed to zero. For the values of the three CPV observables and the corresponding theoretical uncertainties, we follow the calculations in [6, 60].

The fit result is shown as Fig. 19, presenting the projected frequentist interpretations of the NP contributions given the future Tera- Z factory sensitivity. To obtain the contours, for each point in the 2D plane shown, we evaluate minimum χ^2 value, assuming the observed value of all four observables (BR, \mathcal{A}^Δ , \mathcal{C} , \mathcal{S}) take their corresponding SM predictions. During the process, statistical uncertainties and both systematic uncertainties (theoretical and experimental) are considered. The left and right panel stand for the $C_7^{\prime\text{NP}}$ and C_7^{NP} cases, respectively. In each panel, the new physics contributions to the other operator are set to zero for simplicity. The lighter and darker shaded regions correspond to the 1σ and 2σ allowed regions, respectively. Notably, the CP-violating observables exhibit significant sensitivity to NP contributions associated with $C_7^{\prime\text{NP}}$. It is worth emphasizing that the constraints presented herein are solely derived from the $B_s^0 \rightarrow \phi\gamma$ channel at CEPC Tera-Z, complementary and potentially stronger constraints from other channels such as $B_s^0 \rightarrow \phi\ell^+\ell^-$ are expected [61].

6 Conclusion

The $b \rightarrow s\gamma$ process, being a typical FCNC process, serves as a crucial probe for detecting CP Violation and NP. Especially in the context of future Z factories, its study is highly important for probing new physics beyond the Standard Model. The CEPC, leveraging its high statistics, clean collision environment, and excellent detector performance, offers unique advantages for flavor physics research and is an ideal platform for investigating $b \rightarrow s\gamma$ -related decays.

This study focuses on the FCNC decay $B_s^0 \rightarrow \phi\gamma$ and presents a feasibility study under the CEPC Tera-Z operation scenario. The results demonstrate that CEPC can achieve a relative statistical uncertainty of 0.16%, an improvement of two orders of magnitude compared to existing measurements. The corresponding signal selection efficiency and purity are 44.91% and 76.20%, respectively, and the invariant mass resolution is 95.0 MeV. This precision level lays a solid foundation for the subsequent precise extraction of CP-violating parameters and sensitive searches for NP effects. Accounting for the B_s^0/\bar{B}_s^0 mixing effect, a time-dependent analysis of the $B_s^0 \rightarrow \phi\gamma$ decay was performed, and the mixing-induced CP-violating parameters $\mathcal{A}_{\phi\gamma}^\Delta$, $\mathcal{C}_{\phi\gamma}$, and $\mathcal{S}_{\phi\gamma}$ were extracted. Using central value of LHCb measurement as input, the anticipated precision of these parameters are

$$\begin{aligned}\mathcal{A}_{\phi\gamma}^\Delta &= -0.67 \pm 0.021(\text{stat}) \pm 0.035(\text{syst}), \\ \mathcal{C}_{\phi\gamma} &= 0.11 \pm 0.0092(\text{stat}) \pm 0.0027(\text{syst}), \\ \mathcal{S}_{\phi\gamma} &= 0.43 \pm 0.0096(\text{stat}) \pm 0.0064(\text{syst}).\end{aligned}$$

These anticipated precision provides an opportunity for testing CP-violating mechanism within the SM and searching for NP contributions. Furthermore, the 1σ sensitivity boundaries for NP in this study are found to be $\mathcal{A}_{\phi\gamma}^\Delta < -0.05$ or $\mathcal{A}_{\phi\gamma}^\Delta > 0.15$, $\mathcal{C}_{\phi\gamma} < -0.02$ or $\mathcal{C}_{\phi\gamma} > 0.04$, and $\mathcal{S}_{\phi\gamma} < -0.04$ or $\mathcal{S}_{\phi\gamma} > 0.04$. This implies that even though the CEPC's measurement precision for these CP-violating parameters has not fully reached the SM-predicted level, signs of NP can still be detected if the measured parameter values fall

beyond the bounds quoted above. Notably, the CP-violating observables show particular sensitivity to NP contributions associated with $C_7^{\prime \text{NP}}$.

Additionally, this study conducted a relative detector optimization analysis. By establishing the correlation between the intrinsic resolution of the PID performance and ECAL resolution, it provides guidance for optimizing the design of key CEPC detector subsystems.

In summary, this study systematically demonstrates the CEPC's advantages in the research of $B_s^0 \rightarrow \phi\gamma$ decay and related flavor physics. The projected high precision for both signal reconstruction and CP-violating parameter extraction not only significantly improves the tests of SM flavor physics but also provides a sensitive window to NP effects. Furthermore, detector performance studies provide important input for the technical design of the CEPC experiment, supporting its flavor physics goals. Nevertheless, it is important to acknowledge that such high-precision projected precision of 0.1% is still subject to certain conditions. This paper adopts the fast simulation method and assumes an idealized detector response, while the real detector response will have a certain impact. Background modeling depends on the hadronization model in the generators, and its uncertainties may introduce additional systematic effects. In addition, the calibration accuracy of jet tagging will affect the final measurement precision. These aspects require further study in future work.

Acknowledgements

This work was supported by National Key Program for S&T Research and Development under contract number 2024YFA1610603 and 2022YFA1601901. We also thank Wolfgang Altmannshofer, Yuzhi Che and Chia-Wei Liu for useful discussions.

References

- [1] T. Kumar and B. Mawlong, *Exploring new physics in the FCNC $B_c \rightarrow D_s \nu \bar{\nu}$ channel*, in *Particle Physics and Cosmology in the Himalayas*, 2, 2025 [[2502.20980](#)].
- [2] L. Allwicher, M. Bordone, G. Isidori, G. Piazza and A. Stanzione, *Probing third-generation New Physics with $K \rightarrow \pi \nu \nu^-$ and $B \rightarrow K(*) \nu \nu^-$* , *Phys. Lett. B* **861** (2025) 139295 [[2410.21444](#)].
- [3] LHCb collaboration, *Test of lepton universality with $B^0 \rightarrow K^{*0} \ell^+ \ell^-$ decays*, *JHEP* **08** (2017) 055 [[1705.05802](#)].
- [4] LHCb collaboration, *Test of lepton flavor universality using $B \rightarrow D^{*-} \tau^+ \nu \tau$ decays with hadronic τ channels*, *Phys. Rev. D* **108** (2023) 012018 [[2305.01463](#)].
- [5] S. Halder, *Search for lepton universality violation through $b \rightarrow s \ell^+ \ell^-$ mediated rare decays at Belle II*, Ph.D. thesis, Tata Inst., 2024.
- [6] A. Paul and D.M. Straub, *Constraints on new physics from radiative B decays*, *JHEP* **04** (2017) 027 [[1608.02556](#)].
- [7] P. Ball, G.W. Jones and R. Zwicky, *$b \rightarrow v \gamma$ beyond qcd factorization*, *Phys. Rev. D* **75** (2007) 054004.
- [8] A. Ali, B. Pecjak and C. Greub, *Towards $b \rightarrow v \gamma$ decays at nnlo in scet*, *The European Physical Journal C* **55** (2008) 577–595.

[9] BELLE collaboration, *Observation of $B_s^0 \rightarrow \phi\gamma$ and Search for $B_s^0 \rightarrow \gamma\gamma$ Decays at Belle*, *Phys. Rev. Lett.* **100** (2008) 121801 [[0712.2659](#)].

[10] LHCb collaboration, *Measurement of the ratio of branching fractions $\mathcal{B}(B^0 \rightarrow K^{*0}\gamma)/\mathcal{B}(B_s^0 \rightarrow \phi\gamma)$* , *Phys. Rev. D* **85** (2012) 112013 [[1202.6267](#)].

[11] LHCb collaboration, *Measurement of the ratio of branching fractions $BR(B_0 \rightarrow K^{*0}\gamma)/BR(B_{s0} \rightarrow \phi\gamma)$ and the direct CP asymmetry in $B_0 \rightarrow K^{*0}\gamma$* , *Nucl. Phys. B* **867** (2013) 1 [[1209.0313](#)].

[12] LHCb collaboration, *Measurement of CP-violating and mixing-induced observables in $B_s^0 \rightarrow \phi\gamma$ decays*, *Phys. Rev. Lett.* **123** (2019) 081802 [[1905.06284](#)].

[13] BELLE collaboration, *Search for $B_s^0 \rightarrow \gamma\gamma$ and a measurement of the branching fraction for $B_s^0 \rightarrow \phi\gamma$* , *Phys. Rev. D* **91** (2015) 011101 [[1411.7771](#)].

[14] X. Ai et al., *Flavor Physics at CEPC: a General Perspective*, [2412.19743](#).

[15] CEPC STUDY GROUP collaboration, *CEPC Technical Design Report: Accelerator, Radiat. Detect. Technol. Methods* **8** (2024) 1 [[2312.14363](#)].

[16] BELLE-II collaboration, *The Belle II Physics Book*, *PTEP* **2019** (2019) 123C01 [[1808.10567](#)].

[17] LHCb collaboration, *Physics case for an LHCb Upgrade II - Opportunities in flavour physics, and beyond, in the HL-LHC era*, [1808.08865](#).

[18] LHCb collaboration, *Measurement of the b-quark production cross-section in 7 and 13 TeV pp collisions*, *Phys. Rev. Lett.* **118** (2017) 052002 [[1612.05140](#)].

[19] LHCb collaboration, *Measurement of b hadron fractions in 13 TeV pp collisions*, *Phys. Rev. D* **100** (2019) 031102 [[1902.06794](#)].

[20] LHCb collaboration, *Measurement of the B_c^- meson production fraction and asymmetry in 7 and 13 TeV pp collisions*, *Phys. Rev. D* **100** (2019) 112006 [[1910.13404](#)].

[21] HFLAV collaboration, *Averages of b-hadron, c-hadron, and τ -lepton properties as of 2018*, *Eur. Phys. J. C* **81** (2021) 226 [[1909.12524](#)].

[22] X.-C. Zheng, C.-H. Chang, T.-F. Feng and X.-G. Wu, *QCD NLO fragmentation functions for c or b^- quark to B_c or B_c^* meson and their application*, *Phys. Rev. D* **100** (2019) 034004 [[1901.03477](#)].

[23] L. Li and T. Liu, *$b \rightarrow s\tau^+\tau^-$ physics at future Z factories*, *JHEP* **06** (2021) 064 [[2012.00665](#)].

[24] Y. Wang, S. Descotes-Genon, O. Deschamps, L. Li, S. Chen, Y. Zhu et al., *Prospects for $B_{(s)}^0 \rightarrow \pi^0\pi^0$ and $B_{(s)}^0 \rightarrow \eta\eta$ modes and corresponding CP asymmetries at Tera-Z*, *JHEP* **12** (2022) 135 [[2208.08327](#)].

[25] L. Li, M. Ruan, Y. Wang and Y. Wang, *Analysis of $B_s \rightarrow \phi\nu\nu^-$ at CEPC*, *Phys. Rev. D* **105** (2022) 114036 [[2201.07374](#)].

[26] T. Zheng, J. Xu, L. Cao, D. Yu, W. Wang, S. Prell et al., *Analysis of $B_c \rightarrow \tau\nu_\tau$ at CEPC*, *Chin. Phys. C* **45** (2021) 023001 [[2007.08234](#)].

[27] Y. Che, V. Boudry, H. Videau, M. He and M. Ruan, *Cluster time measurement with CEPC calorimeter*, *Eur. Phys. J. C* **83** (2023) 93 [[2209.02932](#)].

[28] H. Liang, Y. Zhu, Y. Wang, Y. Che, C. Zhou, H. Qu et al., *Jet-Origin Identification and Its Application at an Electron-Positron Higgs Factory*, *Phys. Rev. Lett.* **132** (2024) 221802 [[2310.03440](#)].

[29] Y. Coadou, *Boosted decision trees*, [2206.09645](#).

[30] F. Gaede, *Marlin and lccd—software tools for the ilc*, *Nuclear Instruments and Methods in Physics Research Section A: Accelerators, Spectrometers, Detectors and Associated Equipment* **559** (2006) 177.

[31] CEPC STUDY GROUP collaboration, *CEPC Conceptual Design Report: Volume 2 - Physics & Detector*, [1811.10545](#).

[32] K. Kawagoe et al., *Beam test performance of the highly granular SiW-ECAL technological prototype for the ILC*, *Nucl. Instrum. Meth. A* **950** (2020) 162969 [[1902.00110](#)].

[33] H. Wang, X. Luo, J. Lv, X. Sun and M. Ruan, *Design and cosmic ray measurement of liquid scintillator tungsten slice ECAL for future collider*, *JINST* **20** (2025) P04026.

[34] CEPC CALORIMETER WORKING GROUP collaboration, *A novel high-granularity crystal calorimeter*, *PoS ICHEP2022* (2022) 348.

[35] CEPC STUDY GROUP collaboration, *CEPC Technical Design Report - Reference Detector*, [2510.05260](#).

[36] Y. Zhu, S. Chen, H. Cui and M. Ruan, *Requirement analysis for dE/dx measurement and PID performance at the CEPC baseline detector*, *Nucl. Instrum. Meth. A* **1047** (2023) 167835 [[2209.14486](#)].

[37] PARTICLE DATA GROUP collaboration, *Review of Particle Physics*, *PTEP* **2020** (2020) 083C01.

[38] W. Kilian, T. Ohl and J. Reuter, *WHIZARD: Simulating Multi-Particle Processes at LHC and ILC*, *Eur. Phys. J. C* **71** (2011) 1742 [[0708.4233](#)].

[39] T. Sjöstrand, S. Ask, J.R. Christiansen, R. Corke, N. Desai, P. Ilten et al., *An introduction to PYTHIA 8.2*, *Comput. Phys. Commun.* **191** (2015) 159 [[1410.3012](#)].

[40] T. Suehara and T. Tanabe, *Lcfiplus: A framework for jet analysis in linear collider studies*, *Nuclear Instruments and Methods in Physics Research Section A: Accelerators, Spectrometers, Detectors and Associated Equipment* **808** (2016) 109.

[41] H. Qu, C. Li and S. Qian, *Particle Transformer for Jet Tagging*, [2202.03772](#).

[42] Y. Zhu, H. Liang, Y. Wang, Y. Che, H. Wang, C. Zhou et al., *Holistic approach and Advanced Color Singlet Identification for physics measurements at high energy frontier*, [2506.11783](#).

[43] D. Atwood, M. Gronau and A. Soni, *Mixing-induced CP asymmetries in radiative B decays in and beyond the standard model*, *Phys. Rev. Lett.* **79** (1997) 185.

[44] J. Peng, M. Zhao, X. Wang, M. Ruan, H. Li and S. Chen, *Prospect for measurement of CP-violating observables in $B_s^0 \rightarrow D_s^\mp K^\pm$ decays at a future Z factory*, *JHEP* **06** (2025) 212 [[2502.11172](#)].

[45] F. Muheim, Y. Xie and R. Zwicky, *Exploiting the width difference in $bs \rightarrow \phi\gamma$* , *Physics Letters B* **664** (2008) 174.

[46] LHCb COLLABORATION collaboration, *Measurement of cp-violating and mixing-induced observables in $B_s^0 \rightarrow \phi\gamma$ decays*, *Phys. Rev. Lett.* **123** (2019) 081802.

- [47] R. Aaij, B. Adeva, M. Adinolfi, Z. Ajaltouni, S. Akar, J. Albrecht et al., *First experimental study of photon polarization in radiative B_s^0 decays*, *Phys. Rev. Lett.* **118** (2017) 021801.
- [48] BABAR COLLABORATION collaboration, *Measurement of time-dependent cp asymmetry in $B^0 \rightarrow K_S^0 \pi^0 \gamma$ decays*, *Phys. Rev. D* **78** (2008) 071102.
- [49] BABAR COLLABORATION collaboration, *Branching fractions and cp -violating asymmetries in radiative b decays to $\eta k\gamma$* , *Phys. Rev. D* **79** (2009) 011102.
- [50] BABAR COLLABORATION collaboration, *Time-dependent analysis of $B^0 \rightarrow K_S^0 \pi^- \pi^+ \gamma$ decays and studies of the $K^+ \pi^- \pi^+$ system in $B^+ \rightarrow K^+ \pi^- \pi^+ \gamma$ decays*, *Phys. Rev. D* **93** (2016) 052013.
- [51] BELLE COLLABORATION collaboration, *Time-dependent cp asymmetries in $B^0 \rightarrow K_s^0 \pi^0 \gamma$ transitions*, *Phys. Rev. D* **74** (2006) 111104.
- [52] BELLE COLLABORATION collaboration, *Measurement of time-dependent cp asymmetries in $B^0 \rightarrow K_S^0 \eta \gamma$ decays*, *Phys. Rev. D* **97** (2018) 092003.
- [53] BELLE COLLABORATION collaboration, *Measurement of the time-dependent cp asymmetries in $B^0 \rightarrow K_S^0 \rho^0 \gamma$ decays*, *Phys. Rev. Lett.* **101** (2008) 251601.
- [54] BELLE COLLABORATION collaboration, *First observation of radiative $B^0 \rightarrow \phi K^0 \gamma$ decays and measurements of their time-dependent cp violation*, *Phys. Rev. D* **84** (2011) 071101.
- [55] W. Altmannshofer and D.M. Straub, *New physics in $b \rightarrow s$ transitions after LHC run 1*, *Eur. Phys. J. C* **75** (2015) 382 [[1411.3161](#)].
- [56] A. Bharucha, D.M. Straub and R. Zwicky, *$B \rightarrow V \ell^+ \ell^-$ in the Standard Model from light-cone sum rules*, *JHEP* **08** (2016) 098 [[1503.05534](#)].
- [57] T. Blake, G. Lanfranchi and D.M. Straub, *Rare B Decays as Tests of the Standard Model*, *Prog. Part. Nucl. Phys.* **92** (2017) 50 [[1606.00916](#)].
- [58] M. Bordone, C. Cornella and J. Davighi, *Precision tests in $b \rightarrow s \ell^+ \ell^-$ ($\ell = e, \mu$) at FCC-ee*, *Eur. Phys. J. C* **85** (2025) 995 [[2503.22635](#)].
- [59] K.G. Chetyrkin, M. Misiak and M. Munz, *Weak radiative B meson decay beyond leading logarithms*, *Phys. Lett. B* **400** (1997) 206 [[hep-ph/9612313](#)].
- [60] M. Artuso, G. Borissov and A. Lenz, *CP violation in the B_s^0 system*, *Rev. Mod. Phys.* **88** (2016) 045002 [[1511.09466](#)].
- [61] T.H. Kwok, Z. Polonsky, V. Lukashenko, J. Aebischer and B. Kilminster, *Time-dependent precision measurement of $b_s^0 \rightarrow \phi \mu^+ \mu^-$ decay at fcc-ee*, 2025.